

Simulation-guided analysis of resonant soft X-ray scattering for determining the microstructure of triblock copolymers

Veronica G. Reynolds,^{a,^} Devon H. Callan,^{b,^} Kumar Saurabh,^c Elizabeth A. Murphy,^{c,d} Kaitlin R. Albanese,^c Yan-Qiao Chen,^{ad} Claire Wu,^b Eliot Gann,^f Craig J. Hawker,^{a,c,d} Baskar Ganapathysubramanian,^e Christopher M. Bates,^{a,b,c,d} Michael L. Chabinyc^a

^aMaterials Department, ^bDepartment of Chemical Engineering, ^cDepartment of Chemistry & Biochemistry, ^dMaterials Research Laboratory, University of California, Santa Barbara, Santa Barbara, CA 93106, United States, ^eDepartment of Mechanical Engineering, Iowa State University, Ames, IA 50011, United States, ^fMaterials Measurement Laboratory, National Institute of Standards and Technology, Gaithersburg, MD 20899, United States [^]These authors contributed equally.

* To whom correspondence should be addressed: mchabinyc@engineering.ucsb.edu

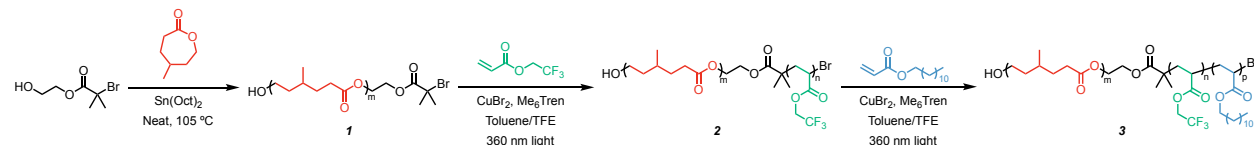
Experimental methods

Materials

All reagents were used as received except where noted. Toluene and copper (II) bromide (CuBr_2) were purchased from Sigma Aldrich.* Dodecyl acrylate (DDA), 2,2,2-trifluoroethyl acrylate (TFEA), and 2,2,2-trifluoroethanol (TFE) were purchased from TCI chemicals. Tris[2-(dimethylamino)ethyl]amine (Me_6Tren) was obtained from Alfa Aesar. Tin(II) 2-ethylhexanoate ($\text{Sn}(\text{Oct})_2$, Aldrich) was fractionally distilled 3 \times under reduced pressure (6.7 Pa, 150 °C) and stored in a nitrogen filled glovebox before use. 4-methylcaprolactone (4MCL) was prepared according to literature, purified by fractional distillation 3 \times from calcium hydride (CaH_2 , Fisher Scientific, 93%), from $\text{Sn}(\text{Oct})_2$ under reduced pressure (6.7 Pa, 50 °C), and stored in a nitrogen filled glovebox before use.¹ Monomers were passed through a column of basic alumina to remove inhibitor prior to use.

Molecular characterization

^1H nuclear magnetic resonance (NMR) spectra were recorded on a Varian VNMRS 600 MHz spectrometer and a Bruker 500 MHz spectrometer. Chemical shifts (δ) are reported in parts per million (ppm) relative to residual CHCl_3 (7.26 ppm). The photo-induced atom-transfer radical polymerization (ATRP) light source (UV: $\lambda_{\text{max}} \approx 360$ nm) was a commercial nail curing lamp (Thermal Spa, obtained online from Amazon) equipped with 3 \times 16 W bulbs.



Scheme S1. Synthesis of P4MCL homopolymer (**1**), P4MCL-*b*-PTFEA diblock copolymer (**2**), and P4MCL-*b*-PTFEA-*b*-PDDA triblock terpolymer (**3**).

Synthesis of poly(4-methyl caprolactone) (P4MCL) homopolymer

Synthesis of the initiator, 2-hydroxyethyl 2-bromoisobutyrate (HEBIB), was implemented according to a reported literature procedure.² In a nitrogen filled glovebox, 4-methyl caprolactone (5.0 g, 39 mmol), HEBIB (7.4 mg, 35 mmol), and $\text{Sn}(\text{Oct})_2$ (7.9 mg, 0.020 mmol) were added to a microwave vial. The vial was sealed, taken out of the glovebox, and placed in a 105 °C oil bath until 70% conversion was achieved, as monitored by ^1H NMR. The vial was quenched in an ice bath to stop the reaction. The viscous mixture was dissolved in a minimal amount of dichloromethane and precipitated into cold methanol (500 mL \times 3). The final product was obtained by drying the precipitate under vacuum for 12 h. ^1H NMR (600 MHz, CDCl_3) δ 4.13 – 4.04 (m, 216H), 2.35 – 2.23 (m, 218H), 1.92 (s, 6H), 1.66 (m, 218H), 1.59 – 1.53 (m, 109H), 1.45 (m, 219H), 0.90 (d, $J = 6.6$ Hz, 330H).

Synthesis of poly(4-methyl caprolactone)-b-poly(2,2,2-trifluoroethyl acrylate) (P4MCL-b-PTFEA) diblock copolymer

A solution of CuBr₂ (2.4 mg, 0.011 mmol) and Me₆Tren (17 μL, 0.063 mmol) was prepared in 2 mL of TFE and sonicated for thirty minutes. In a scintillation vial, previously prepared P4MCL homopolymer (0.51 g, 0.04 mmol) was added and dissolved in 2.1 mL of toluene. TFEA (0.78 g, 3.7 mmol) and 0.49 mL of the TFE stock solution were added to the vial. The solution was degassed with nitrogen for fifteen minutes. With stirring, the polymerization mixture was irradiated ($\lambda \approx 360$ nm) in a commercial UV nail lamp until 60% conversion was achieved, as monitored by ¹H NMR. The viscous mixture was diluted with dichloromethane, filtered through basic alumina to remove residual copper, and dried under vacuum for 12 h to obtain the desired diblock copolymer. ¹H NMR (600 MHz, CDCl₃) δ 4.54 – 4.40 (m, 167H), 4.17 – 4.04 (m, 215H), 2.46 (m, 81H), 2.38 – 2.23 (m, 225H), 2.06 (m, 37H), 1.82 – 1.72 (m, 89H), 1.72 – 1.63 (m, 228H), 1.62 – 1.53 (m, 138H), 1.52 – 1.42 (224H), 1.19 – 1.11 (m, 6H), 0.92 (d, $J = 6.6$ Hz, 2H).

Synthesis of poly(4-methyl caprolactone)-b-poly(2,2,2-trifluoroethyl acrylate)-b-poly(dodecyl acrylate) (P4MCL-b-PTFEA-b-PDDA) triblock copolymer

A solution of CuBr₂ (2.4 mg, 0.011 mmol) and Me₆Tren (17 μL, 0.063 mmol) was prepared in 2 mL of TFE and sonicated for thirty minutes. In a scintillation vial, previously prepared P4MCL-b-PTFEA diblock copolymer (0.64 g, 0.02 mmol) was added and dissolved in 4 mL of toluene. DDA (0.26 g, 1.1 mmol), 0.48 mL of the TFE stock solution, and an additional 0.5 mL TFE were added to the vial. The solution was degassed with nitrogen for fifteen minutes. With stirring, the polymerization mixture was irradiated ($\lambda \approx 360$ nm) in a commercial UV nail lamp until 50% conversion was achieved as monitored by ¹H NMR. The viscous mixture was purified via dissolution in a minimal amount of dichloromethane and precipitated into cold methanol (200 mL x3). The final product was obtained by drying the precipitate under vacuum for 12 h. ¹H NMR (600 MHz, CDCl₃) δ 4.52 – 4.38 (m, 168H), 4.15 – 4.04 (m, 228H), 4.04 – 3.89 (m, 32H), 2.54 – 2.37 (m, 84H), 2.37 – 2.21 (m, 241H), 2.11 – 1.95 (m, 39H), 1.79 – 1.71 (m, 89H), 1.71 – 1.61 (m, 252H), 1.61 – 1.50 (m, 129H), 1.45 (m, 236H), 1.33 – 1.19 (m, 349H), 0.90 (d, $J = 6.6$ Hz, 329H), 0.86 (t, $J = 7.1$ Hz, 63H).

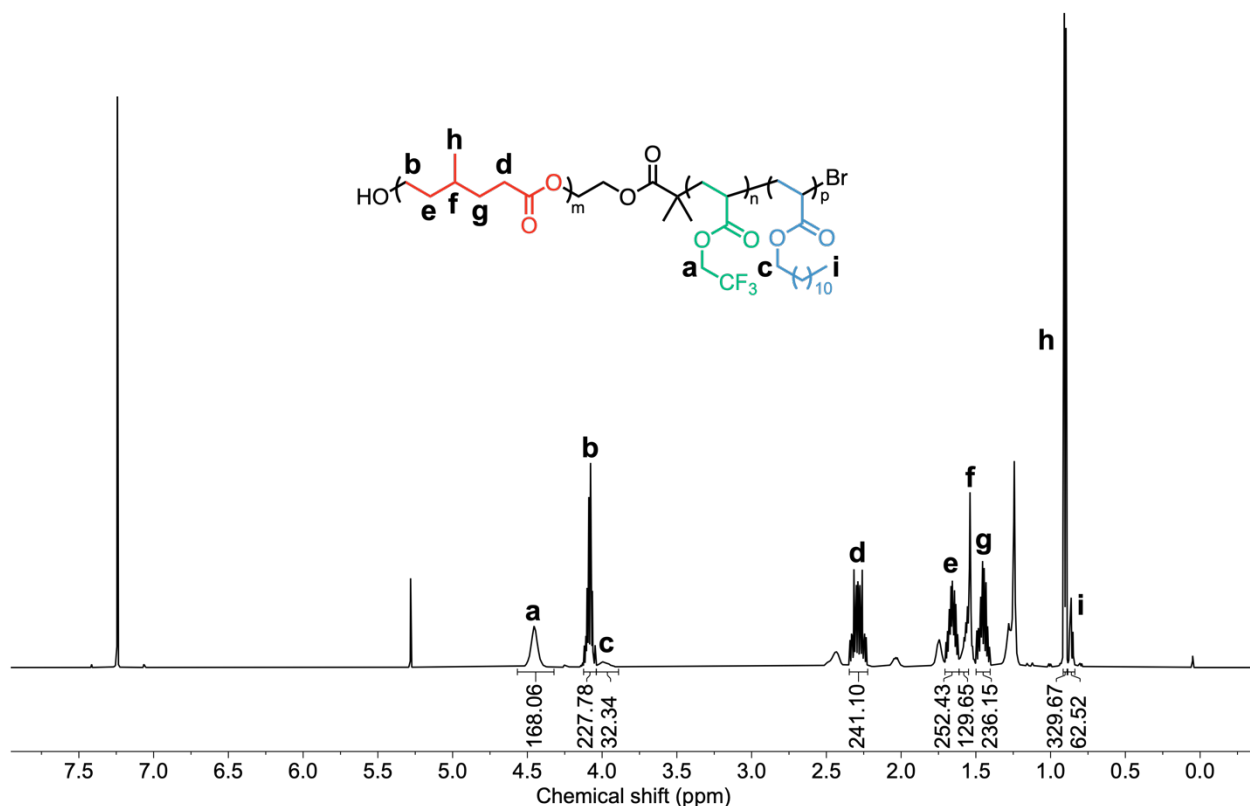


Figure S1. ¹H NMR of P4MCL-*b*-PTFEA-*b*-PDDA triblock terpolymer in CDCl₃.

Synthesis of poly(2,2,2-trifluoroethyl acrylate) homopolymer (PTFEA)

For the following experiment, a stock solution of copper(II) bromide (14.0 mg, 0.062 mmol) and Me₆Tren (8.6 mg, 100 μL, 37.4 mmol) in 1 mL of trifluoroethanol (TFE) and sonicated until complete dissolution. TFEA (4.76 g, 30.90 mmol) and 2-hydroxyethyl 2-bromoisobutyrate (70 mg, 0.33 mmol) were added to a scintillation vial containing 4.76 mL TFE and 40 μL of the Cu(II)/TFE stock solution. The vial was capped with a rubber septum and the solution purged with argon for 15 minutes. With stirring, the reaction mixture was irradiated ($\lambda \approx 360$ nm) until 70 % conversion of monomer was achieved as monitored using ¹H NMR through end group analysis. Upon completion, the reaction mixture was run through a basic alumina column and the resulting polymer was isolated as a viscous liquid following purification via precipitation into hexanes. ¹H NMR (500 MHz, CDCl₃) δ 4.62 – 4.40 (m, 125H), 3.88 – 3.78 (m, 2H), 2.48 (s, 61H), 2.09 (m, 29H), 1.79 (m, 63H), 1.70 – 1.56 (m, 32H), 1.21 (dt, $J = 22.6, 2.4$ Hz, 6H).

*Synthesis of poly(lactide)-b-poly(2,2,2-trifluoroethyl acrylate) diblock copolymer (PLA-*b*PTFEA)*

In a nitrogen filled glove box, (\pm) lactide (0.58 g, 3.86 mmol), triethylaluminum (0.05 M, 520 μL) and mL toluene were added to a microwave vial containing previously prepared PTFEA

(0.50 g, 0.05 mmol, $M_{n,NMR} = 9700$ kg/mol). The vial was sealed with a crimp cap and the reaction was heated to 90 °C in an oil bath for 2.5 h (80% conv.) and subsequently quenched with hydrochloric acid (1M, 0.2 mL). The resulting diblock was isolated via precipitation in MeOH (50 mL, x3). $^1\text{H NMR}$ (500 MHz, CDCl_3) δ 5.31 – 5.12 (m, 93H), 4.50 (m, 6.0 Hz, 125H), 2.58 – 2.41 (m, 60H), 2.07 (m, 28H), 1.79 (m, 63H), 1.67 – 1.53 (m, 308H).

Fractionation of P4MCL-b-PTFEA-b-PDDA triblock via automated flash chromatography

Automated flash chromatography was performed using a Biotage Isolera One purification system equipped with an evaporative light scattering detector (ELSD). A Biotage SNAP KP-Sil 50 g cartridge was used with a flow rate of 40 mL/min. The parent block copolymer was dissolved in hexanes and loaded onto a samplet using a syringe. The screw-top cap was then removed and the samplet was dried at 60 °C overnight. The column was equilibrated with three column volumes of hexanes. After equilibration was complete, the solvent dispersant head insert was detached and the loaded samplet was inserted. The parent block copolymer was eluted with a programmed hexanes/ethyl acetate gradient. All chromatographic solvents were ACS grade or better and used without further purification. Fractions were monitored by a light scattering detector and collected in 15 mL increments. Volume fractions of the fractionated materials were calculated by $^1\text{H NMR}$ by comparing the integrations of the three blocks to their respective homopolymer densities at 25 °C.

Synthesis of poly(2,2,2-trifluoroethyl acrylate) homopolymer (PTFEA)

For the following experiment, a stock solution of copper(II) bromide (14.0 mg, 0.062 mmol) and Me_6Tren (8.6 mg, 100 μL , 37.4 mmol) in 1 mL of trifluoroethanol (TFE) and sonicated until complete dissolution. TFEA (4.76 g, 30.90 mmol) and 2-hydroxyethyl 2-bromoisobutyrate (70 mg, 0.33 mmol) were added to a scintillation vial containing 4.76 mL TFE and 40 μL of the Cu(II)/TFE stock solution. The vial was capped with a rubber septum and the solution purged with argon for 15 minutes. With stirring, the reaction mixture was irradiated ($\lambda \approx 360$ nm) until 70% conversion of monomer was achieved as monitored using $^1\text{H NMR}$ through end group analysis. Upon completion, the reaction mixture was run through a basic alumina column and the resulting polymer was isolated as a viscous liquid following purification via precipitation into hexanes.

Synthesis of poly(lactide)-b-poly(2,2,2-trifluoroethyl acrylate) diblock copolymer (PLA-b-PTFEA)

In a nitrogen filled glove box, (\pm) lactide (0.58 g, 3.86 mmol), triethylaluminum (0.05 M, 520 μL) and mL toluene were added to a microwave vial containing previously prepared PTFEA (0.50 g, 0.05 mmol, $M_{n,NMR} = 9700$ kg/mol). The vial was sealed with a crimp cap and the reaction was heated to 90 °C in an oil bath for 2.5 h (80% conv.) and subsequently quenched with hydrochloric acid (1 M, 0.2 mL). The resulting diblock was isolated via precipitation in

MeOH (50 mL, x3). ^1H NMR (500 MHz, CDCl_3) δ 5.32 – 5.10 (m, 92H), 4.60 – 4.39 (m, 125H), 2.48 (s, 61H), 2.08 (s, 28H), 1.79 (d, $J = 7.6$ Hz, 62H), 1.59 (s, 308H).

*Certain commercial equipment, instruments, software, suppliers or materials are identified in this paper to foster understanding. Such identification does not imply recommendation or endorsement by the National Institute of Standards and Technology, nor does it imply that the materials or equipment identified are necessarily the best available for the purpose.

Optical microscopy of thin films for NEXAFS measurements

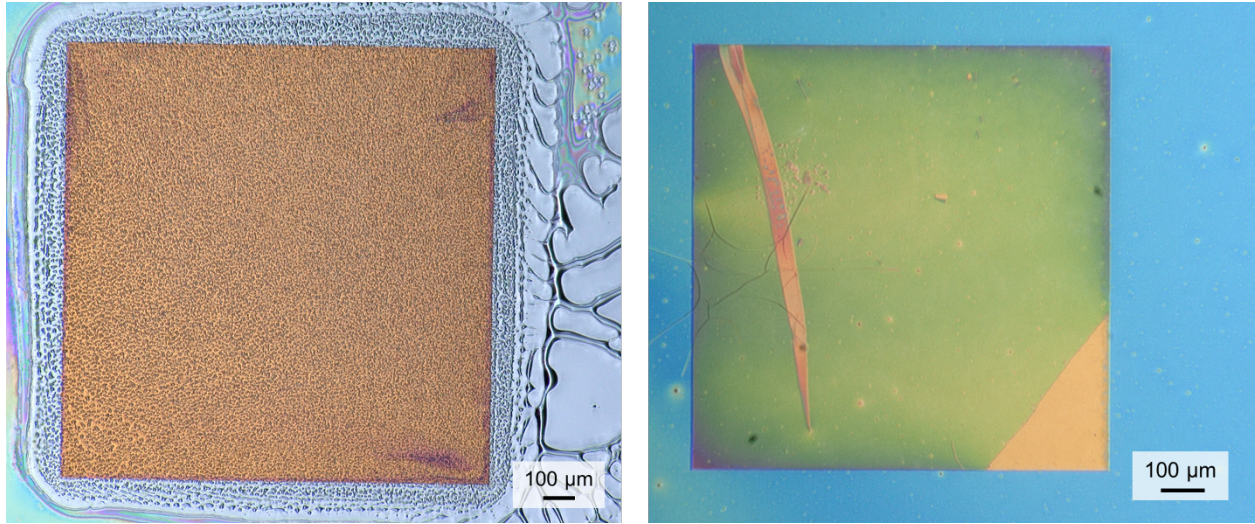


Figure S2. *Left:* Optical micrograph of PTFEA homopolymer dewetted from a silicon nitride substrate after spin coating. The sample was spin coated from 0.03 mass fraction solution in 2,2,2-trifluoroethanol (TFE) (10 μL , 45 s, 1500 acceleration, 2500 revolutions per minute, RPM). *Right:* Optical micrograph of a PLA-*b*-PTFEA diblock thin film on a silicon nitride substrate. The diblock thin film was spin coated from 0.05 mass fraction solution in chlorobenzene (60 μL , 45 s, 1500 acceleration, 2500 RPM) onto a quartz substrate. The film was then floated off of the quartz substrate using a bath of deionized water and transferred to the silicon nitride substrate.

Refractive index of mixtures calculation

The equations below show the calculation of the refractive index of block A from the measured refractive index of an AB diblock, using the known refractive index of block B and the assumption that the refractive index of the diblock is a volume-fraction average. This analysis assumes the components do not interact electronically such that the spectra are additive.³ In the equations below, \hat{n} is the complex index of refraction ($\hat{n} = 1 - \delta + i\beta$) and ϕ is the volume fraction.

$$\hat{n} = \sum_i \phi_i \hat{n}_i$$

$$\delta_A = \frac{1}{\phi_A} (\delta_{diblock} - \phi_B \delta_B)$$

$$\beta_A = \frac{1}{\phi_A} (\beta_{diblock} - \phi_B \beta_B)$$

We additionally assumed that density is a volume-fraction average ($\rho_{diblock} = \phi_A \rho_A + \phi_B \rho_B$, where ρ is density).

Complex refractive indices of P4MCL, PTFEA, and PDDA

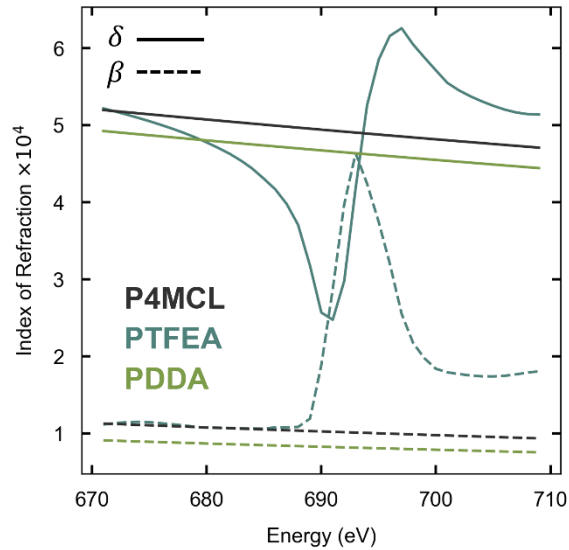


Figure S3. The real (δ) and imaginary (β) components of the complex index of refraction for the three block chemistries. The optical constants for P4MCL and PDDA were estimated using the Henke atomic scattering factors, while those for PTFEA were measured by transmission NEXAFS.

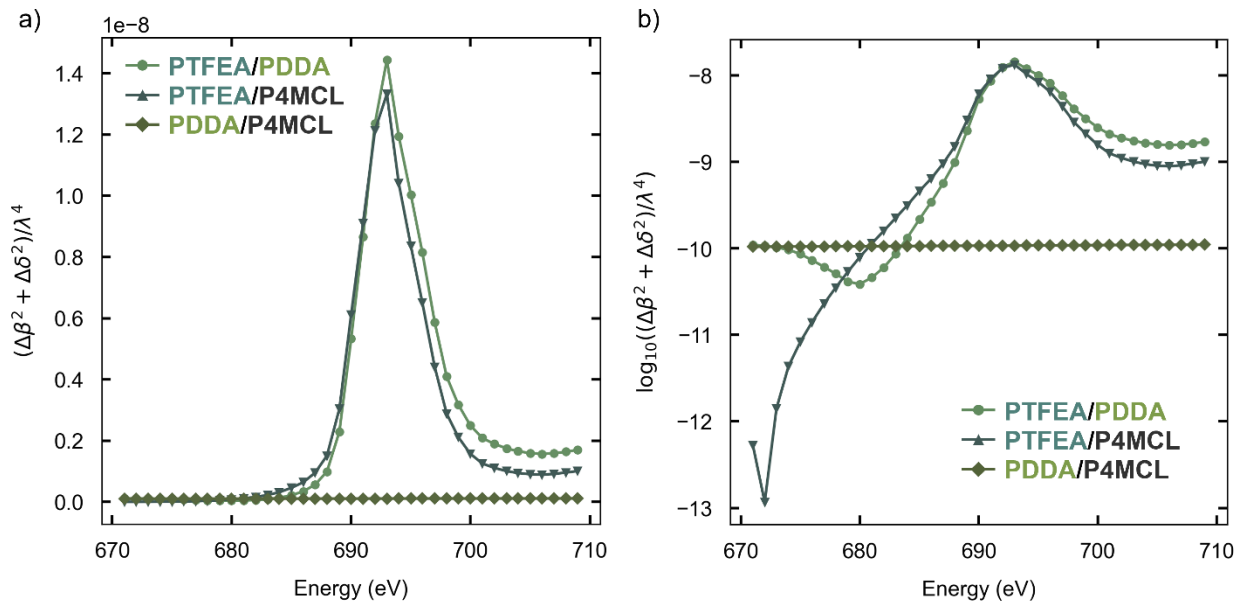


Figure S4. a) Pairwise contrast functions $((\Delta\beta^2 + \Delta\delta^2)/\lambda^4)$ of PTFEA, PDDA, and P4MCL over the fluorine edge. b) Logarithm of the pairwise contrast functions. The contrast between PDDA and P4MCL stays roughly constant on the order of 10^{-10} , while the contrast between PTFEA and the other two has a maximum on the order of 10^{-8} from fluorine resonance. The PTFEA and P4MCL are contrast-matched around 672 eV.

Geometric derivations for microstructure models

Dimensional calculations for hexagonally-packed cylinder morphologies using the scattering-derived d -spacing and the NMR-derived volume fractions.

d : d -spacing

a : lattice parameter

$A_{unit\ cell}$: area of the unit cell

$$d = \frac{2\pi}{q^*}$$

$$a = \frac{2}{\sqrt{3}}d$$

$$A_{unit\ cell} = a^2 \cos 30^\circ$$

I. Core-Shell Cylinders

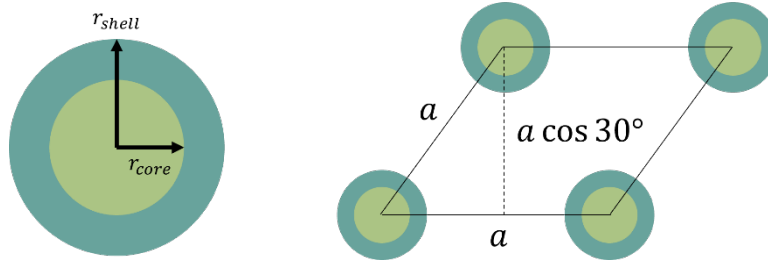


Figure S5. Schematic for the derivation of core-shell dimensions.

Derivation of r_{core} and r_{shell} (note that r_{shell} is defined as the distance from the center of the core-shell cylinder; the shell thickness $t_{shell} = r_{shell} - r_{core}$):

f_{core} : volume fraction of the core material

f_{shell} : volume fraction of the shell material

f_{matrix} : volume fraction of the matrix material

$$f_{core} + f_{shell} + f_{matrix} = 1$$

$$A_{core-shell} = (f_{core} + f_{shell}) \cdot A_{unit\ cell}$$

$$r_{shell} = \sqrt{\frac{A_{core-shell}}{\pi}}$$

$$\frac{A_{core}}{A_{core-shell}} = \frac{f_{core}}{f_{core} + f_{shell}}$$

$$r_{core} = \sqrt{\frac{A_{core}}{A_{core-shell}}} \cdot r_{shell}$$

II. Nested Lattices

Derivation of r_1 (larger spacing sub-lattice, green) and r_2 (smaller spacing sub-lattice, blue):

f_1 : volume fraction of the sub-lattice #1 material (green)

f_2 : volume fraction of the sub-lattice #2 material (blue)

f_{matrix} : volume fraction of the matrix material

$$f_1 + f_2 + f_{matrix} = 1$$

In the nested lattices case, we define the unit cell as:

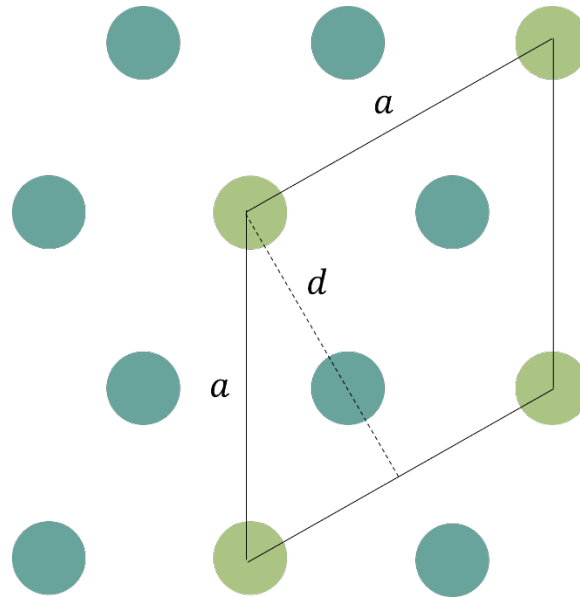


Figure S6. Schematic for the derivation of nested lattices dimensions.

There is one full cylinder of the material on sub-lattice #1 in the unit cell (green). There are 2 full cylinders of the material on sub-lattice #2 in the unit cell (blue).

$$r_1 = \sqrt{\frac{f_1 \cdot A_{unit\ cell}}{\pi}}$$

$$r_2 = \sqrt{\frac{f_2 \cdot A_{unit\ cell}}{2\pi}}$$

Data reduction & peak fitting

The 2D scattering patterns were reduced to 1D line profiles using Nika, an Igor Pro-based package for SAXS/WAXS data reduction.⁴ The sample-to-detector distance was calibrated using a silver behenate standard.

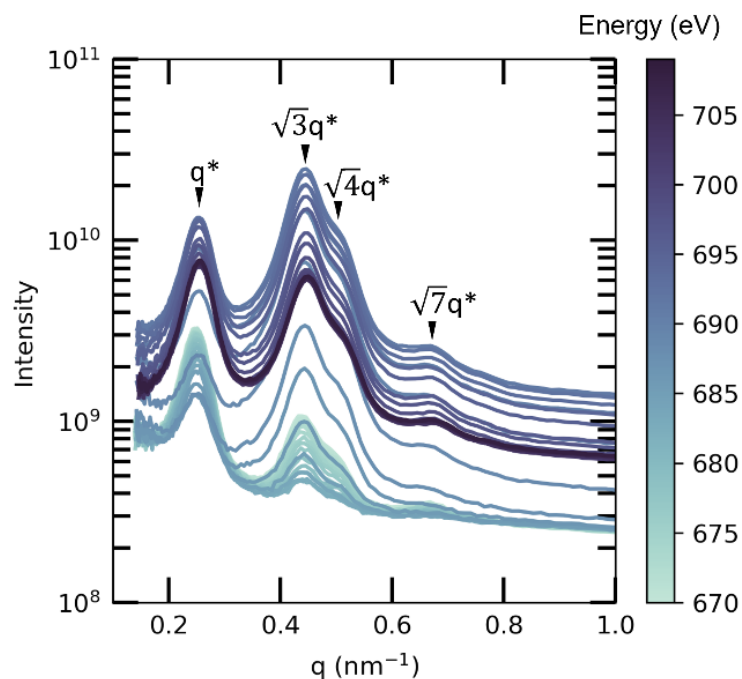


Figure S7. Radially-averaged resonant soft X-ray scattering profiles of P4MCL-*b*-PTFEA-*b*-PDDA collected across the fluorine edge.

One challenge in extracting peak intensity ratios from the experimental RSoXS dataset is the selection and fit of an appropriate baseline. The experimental data were fit using 3 Gaussian peaks and a cubic polynomial baseline. The fitting was performed using lmfit, an open-source Python package.⁵ The baseline was allowed to vary across energies (but kept consistent for a single energy). For the peaks, σ was kept constant ($\sigma_{q^*} = 0.023$, $\sigma_{\sqrt{3}q^*} = 0.027$, $\sigma_{\sqrt{4}q^*} = 0.022$) while the amplitude was allowed to vary. The q^* and $\sqrt{3}q^*$ peak centers were generally allowed to vary and remained consistent, within < 3% variation. Due to the convoluted nature of the $\sqrt{3}q^*$ and $\sqrt{4}q^*$ peaks and the relatively low intensity of the $\sqrt{4}q^*$ at certain energies, the $\sqrt{4}q^*$ peak center was held constant relative to the $\sqrt{3}q^*$ peak center.

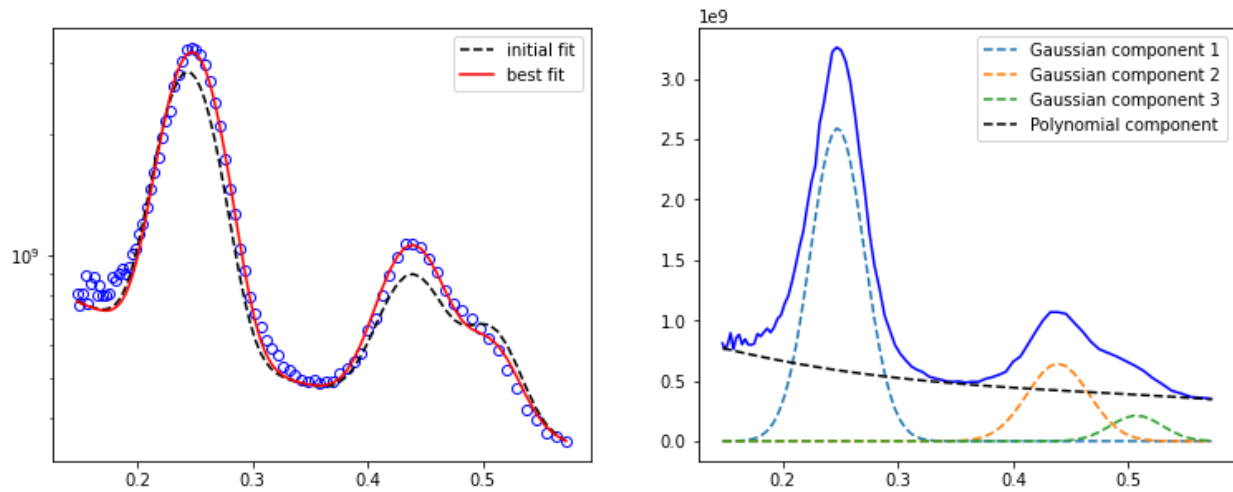


Figure S8. Example fit of a cubic polynomial baseline and 3 Gaussian peaks at 670 eV.

CS1

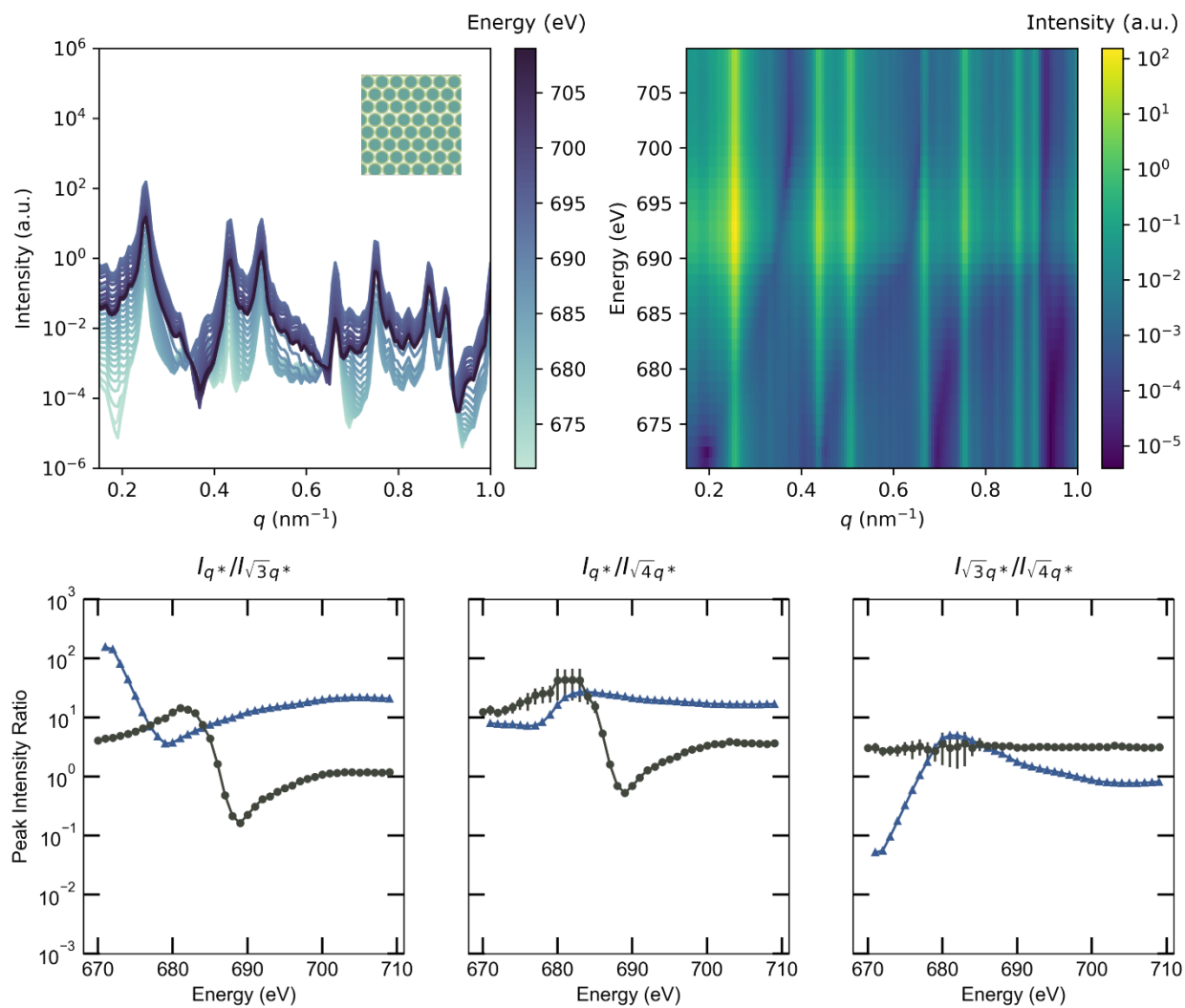


Figure S9. Scattering simulation results for CS1. *Top left:* Radially-averaged simulated RSoXS profiles at energies along the F edge (*inset:* 200×200 voxel subset of the model); *Top right:* intensity map of the simulated RSoXS profiles; *Bottom:* energy dependence of peak intensity ratios (dark grey circles: experiment; blue triangles: simulation).

CS2

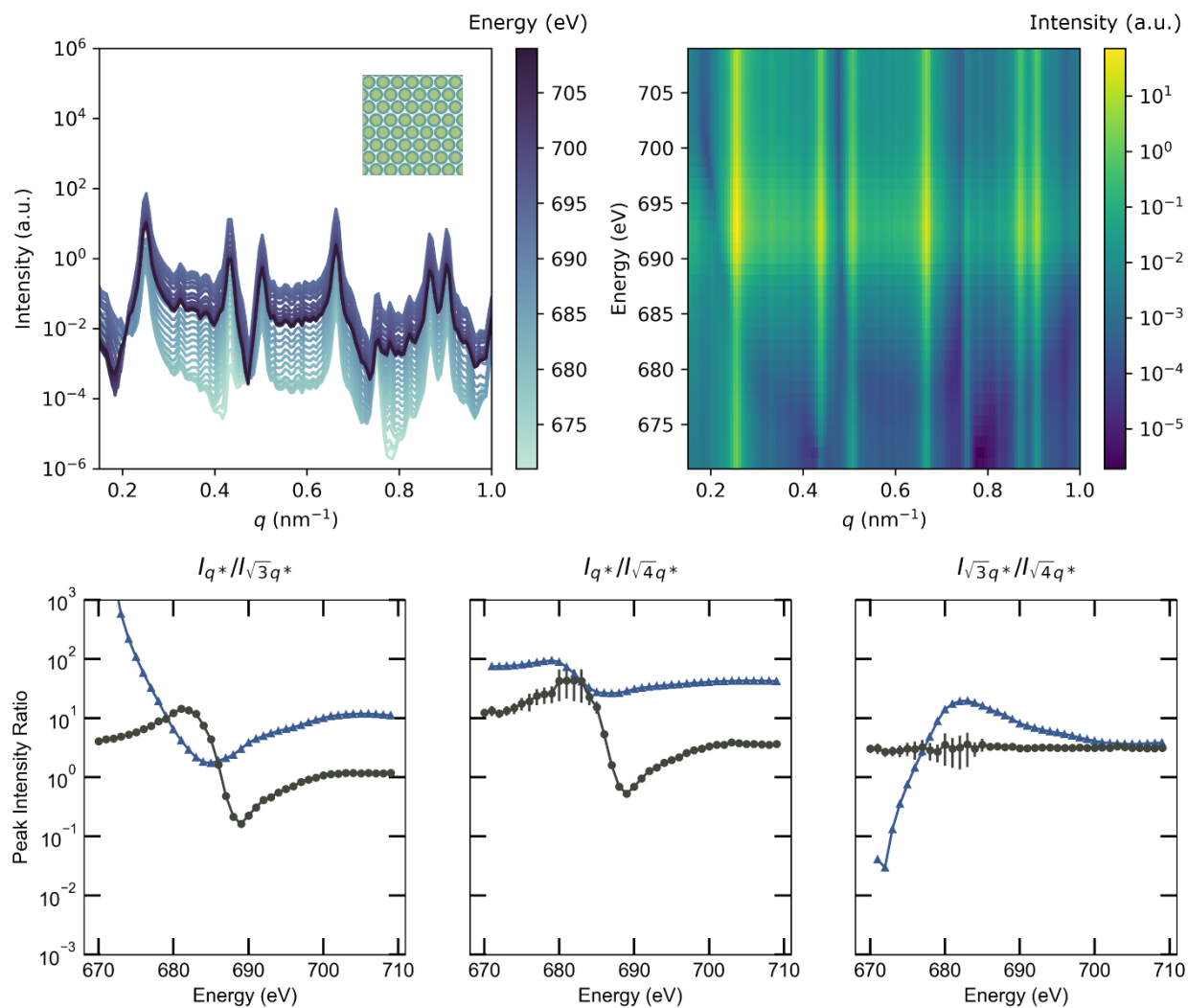


Figure S10. Scattering simulation results for CS2. *Top left:* Radially-averaged simulated RSoXS profiles at energies along the F edge (*inset:* 200 × 200 voxel subset of the model); *Top right:* intensity map of the simulated RSoXS profiles; *Bottom:* energy dependence of peak intensity ratios (dark grey circles: experiment; blue triangles: simulation).

CS3

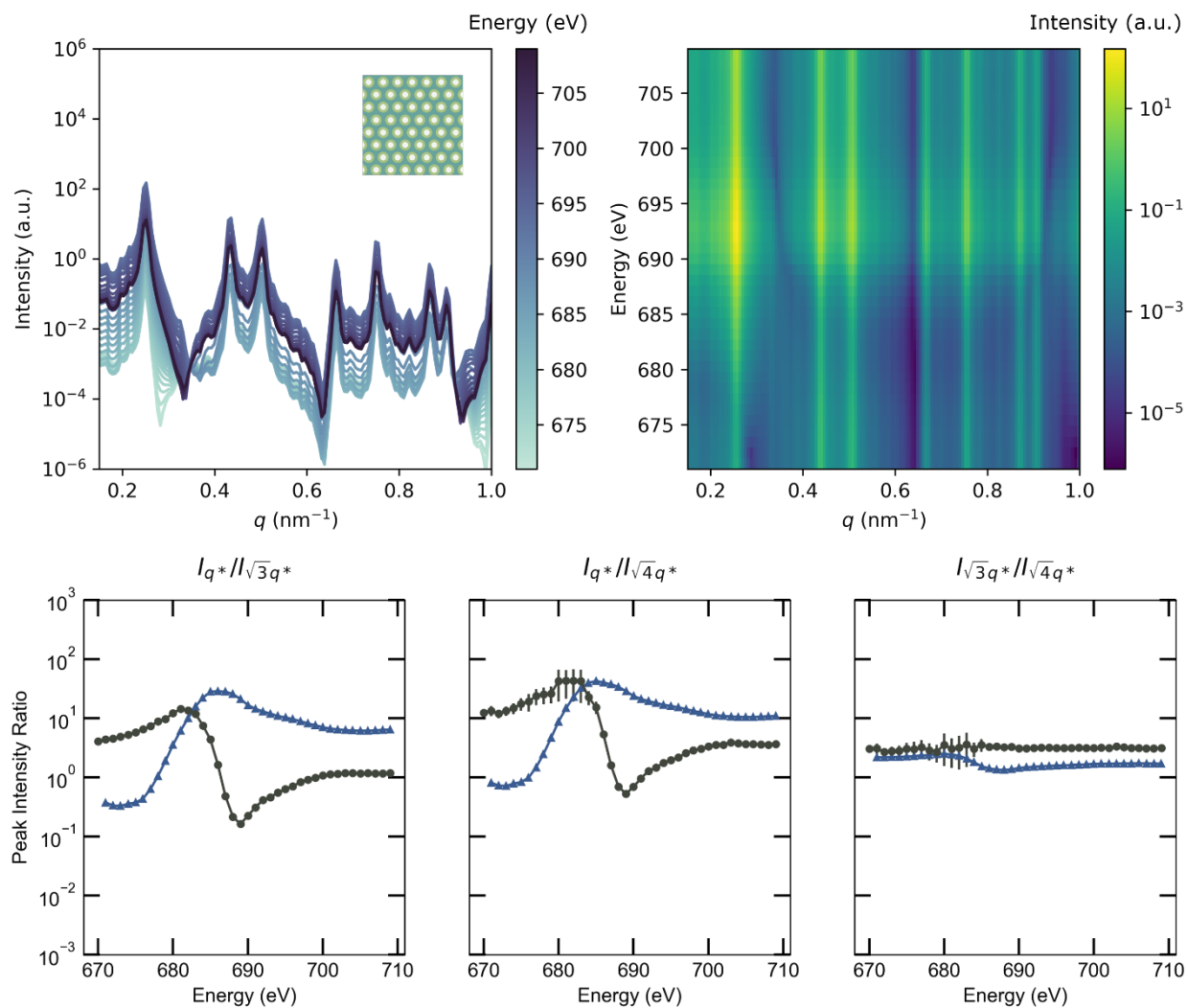


Figure S11. Scattering simulation results for CS3. *Top left:* Radially-averaged simulated RSoXS profiles at energies along the F edge (*inset:* 200×200 voxel subset of the model); *Top right:* intensity map of the simulated RSoXS profiles; *Bottom:* energy dependence of peak intensity ratios (dark grey circles: experiment; blue triangles: simulation).

CS4

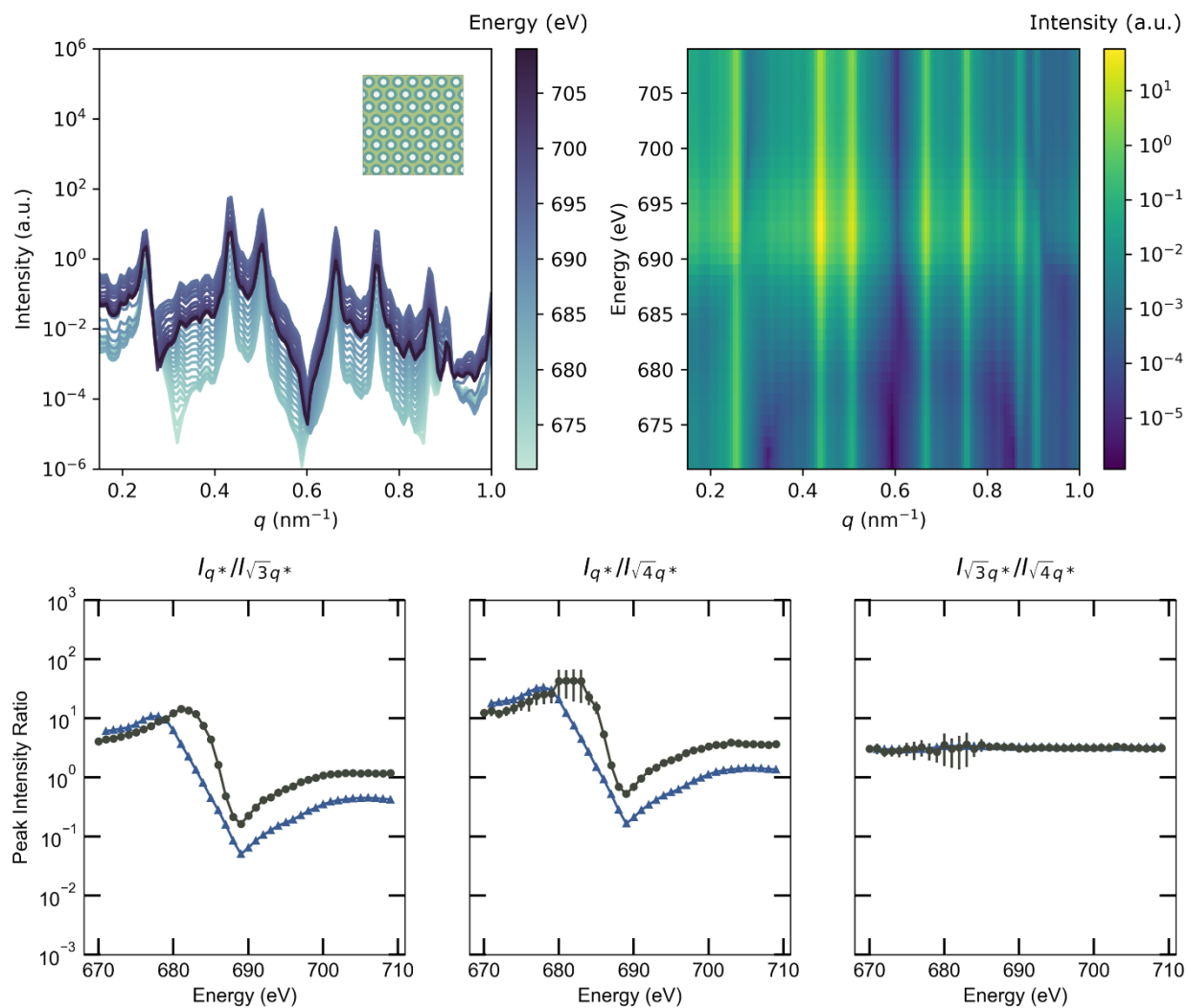


Figure S12. Scattering simulation results for CS4. *Top left:* Radially-averaged simulated RSoXS profiles at energies along the F edge (*inset:* 200×200 voxel subset of the model); *Top right:* intensity map of the simulated RSoXS profiles; *Bottom:* energy dependence of peak intensity ratios (dark grey circles: experiment; blue triangles: simulation).

CS5

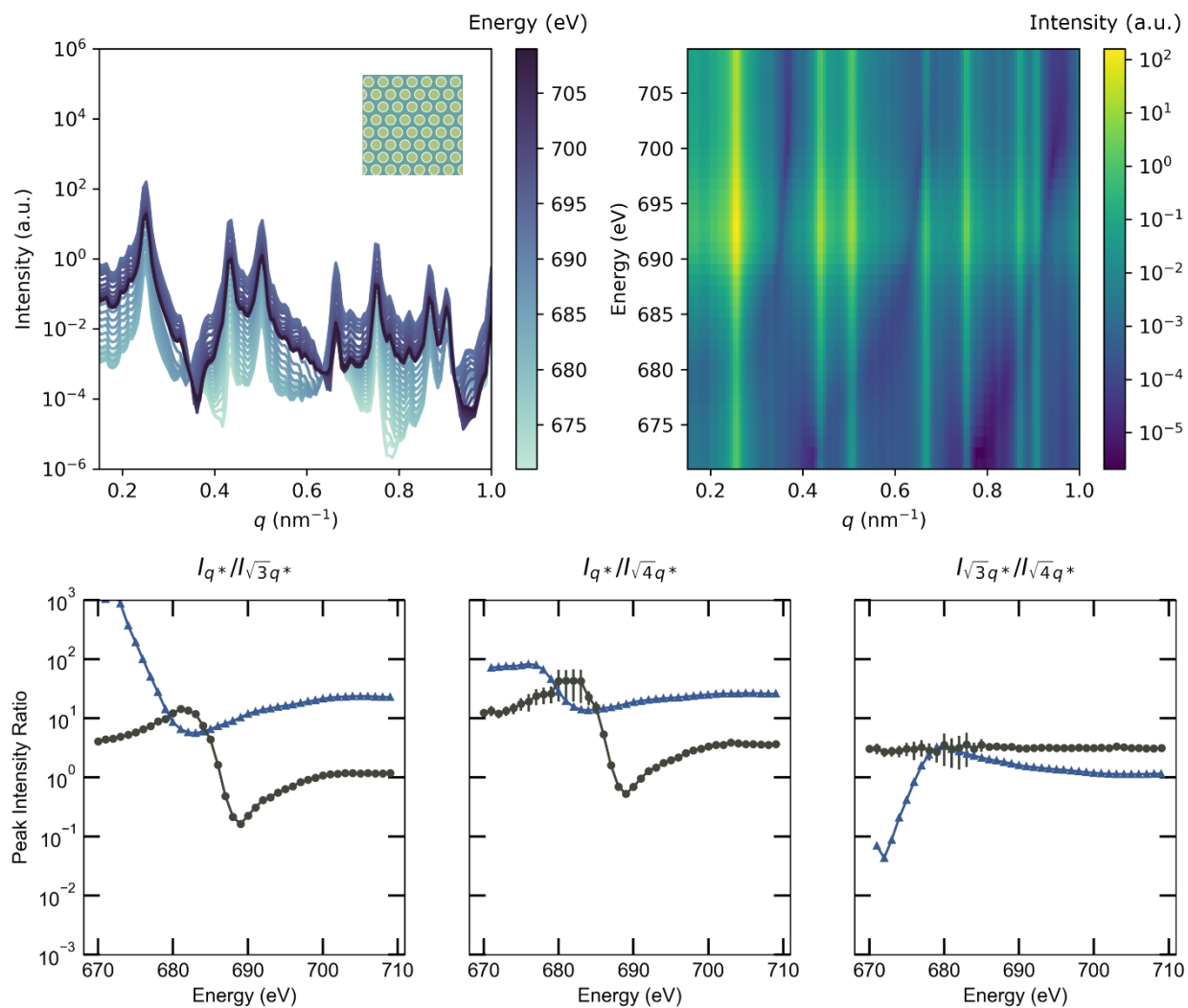


Figure S13. Scattering simulation results for CS5. *Top left:* Radially-averaged simulated RSoXS profiles at energies along the F edge (*inset:* 200×200 voxel subset of the model); *Top right:* intensity map of the simulated RSoXS profiles; *Bottom:* energy dependence of peak intensity ratios (dark grey circles: experiment; blue triangles: simulation).

CS6

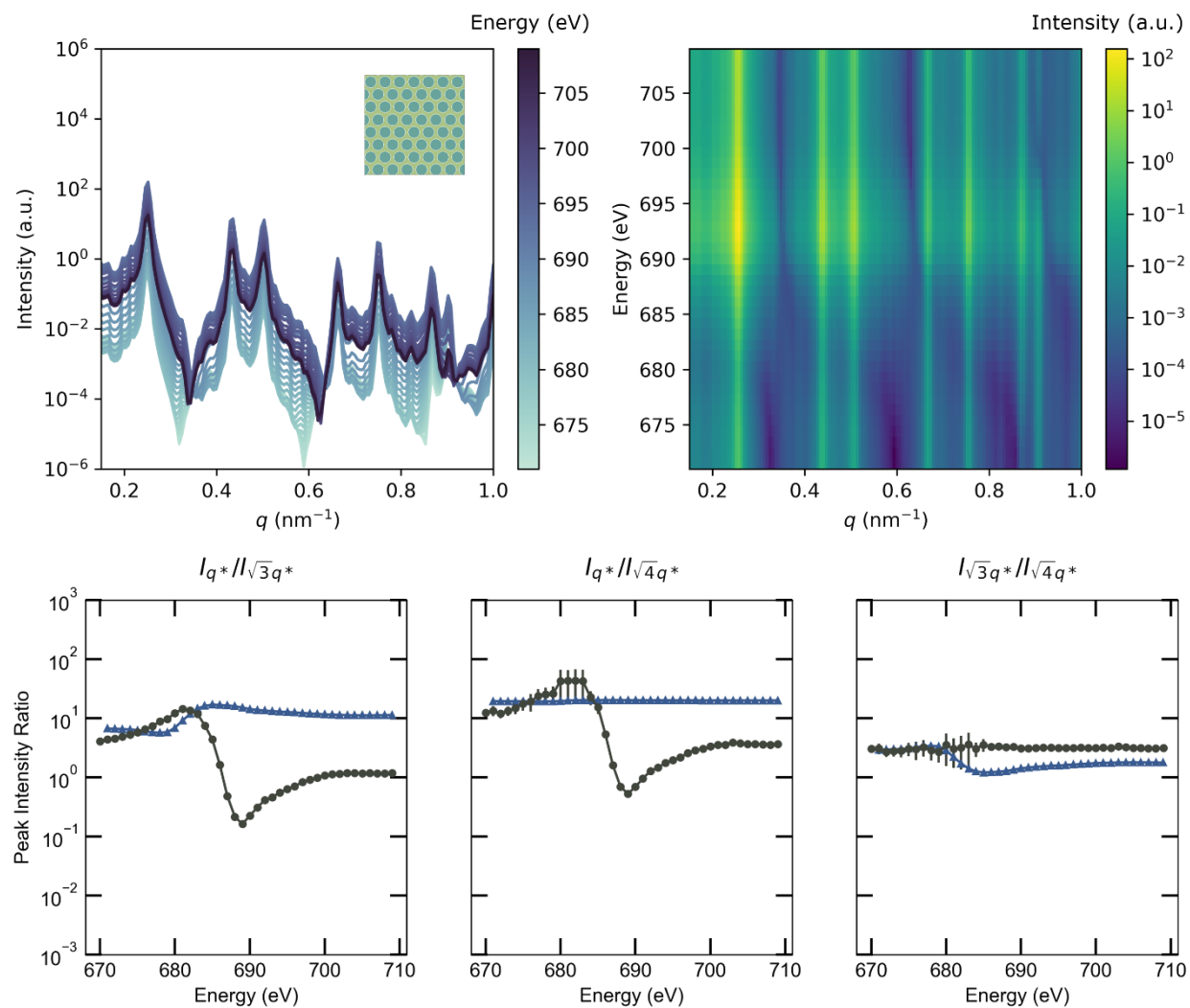


Figure S14. Scattering simulation results for CS6. *Top left:* Radially-averaged simulated RSoXS profiles at energies along the F edge (*inset:* 200×200 voxel subset of the model); *Top right:* intensity map of the simulated RSoXS profiles; *Bottom:* energy dependence of peak intensity ratios (dark grey circles: experiment; blue triangles: simulation).

NL1

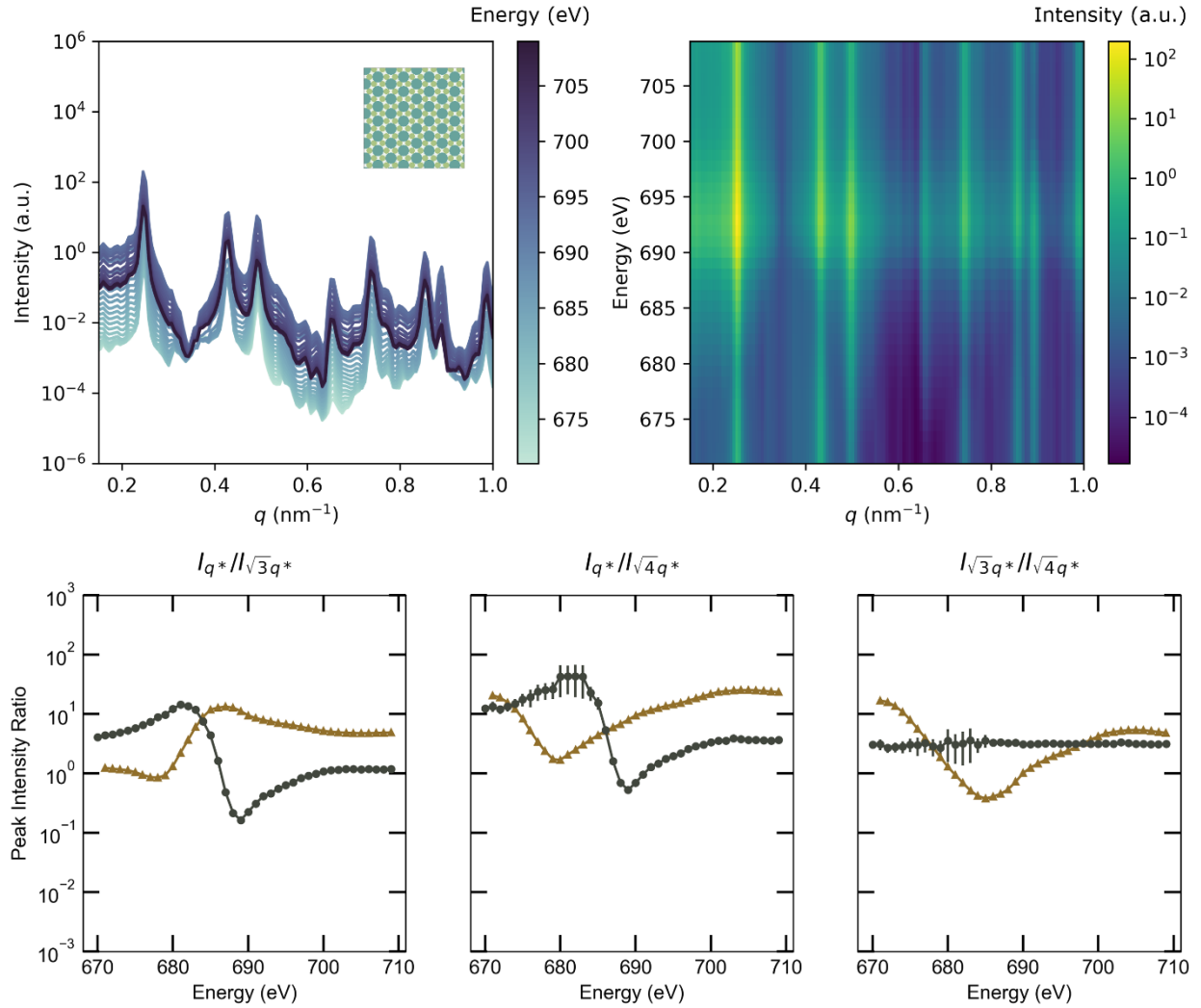


Figure S15. Scattering simulation results for NL1. *Top left:* Radially-averaged simulated RSoXS profiles at energies along the F edge (*inset:* 200 × 200 voxel subset of the model); *Top right:* intensity map of the simulated RSoXS profiles; *Bottom:* energy dependence of peak intensity ratios (dark grey circles: experiment; gold triangles: simulation).

NL2

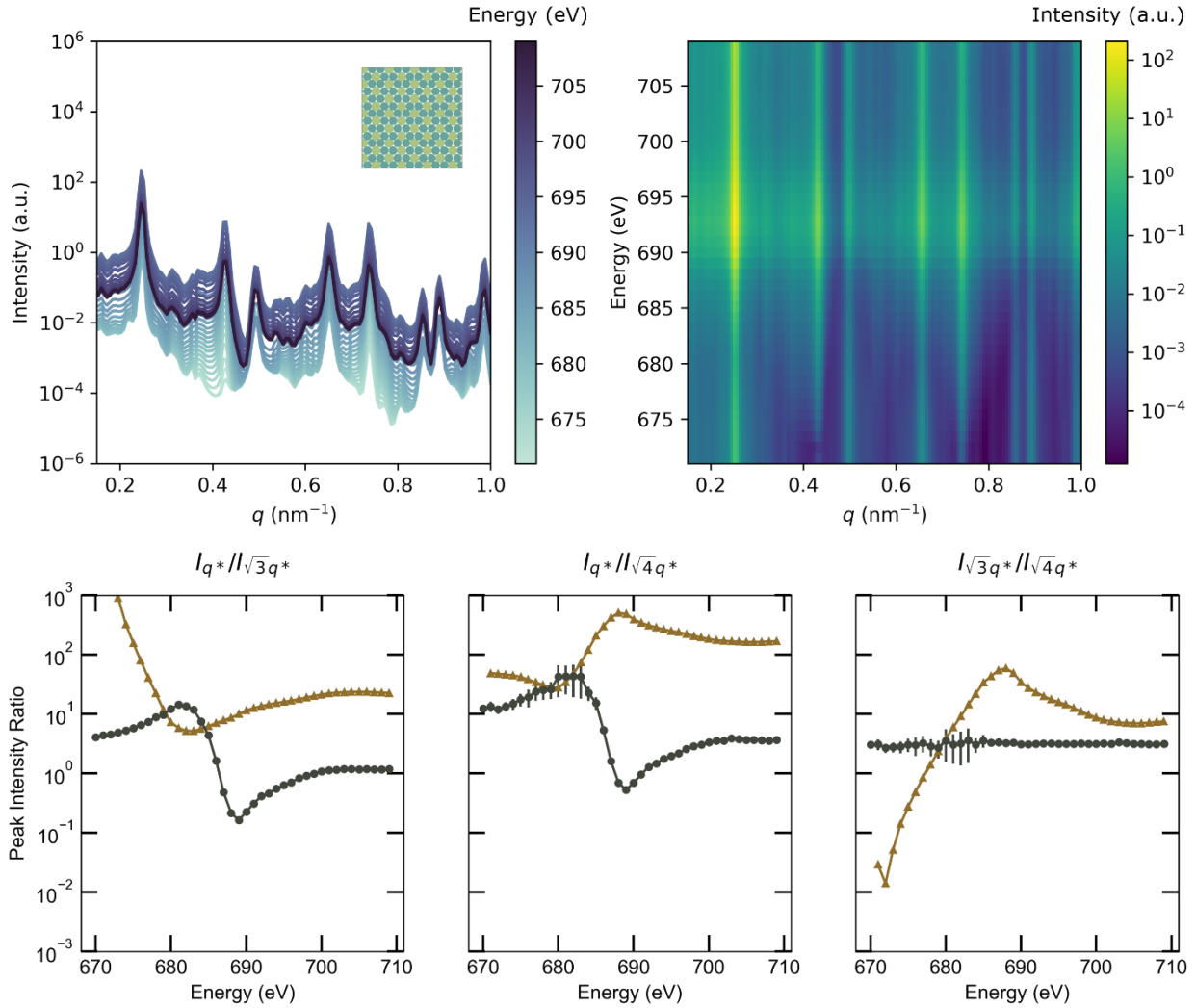


Figure S16. Scattering simulation results for NL2. *Top left:* Radially-averaged simulated RSoXS profiles at energies along the F edge (*inset:* 200 × 200 voxel subset of the model); *Top right:* intensity map of the simulated RSoXS profiles; *Bottom:* energy dependence of peak intensity ratios (dark grey circles: experiment; gold triangles: simulation).

NL3

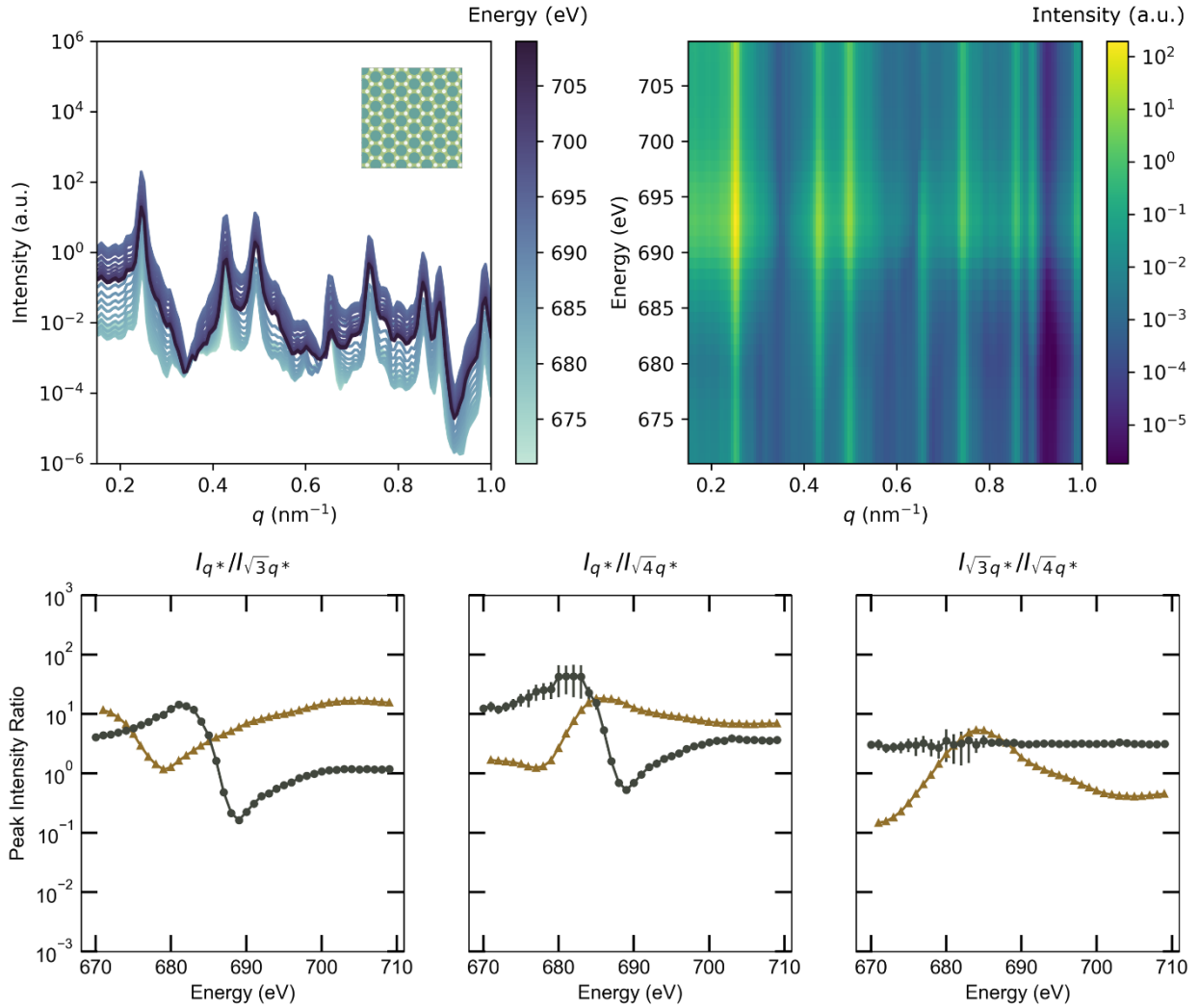


Figure S17. Scattering simulation results for NL3. *Top left:* Radially-averaged simulated RSoXS profiles at energies along the F edge (*inset:* 200×200 voxel subset of the model); *Top right:* intensity map of the simulated RSoXS profiles; *Bottom:* energy dependence of peak intensity ratios (dark grey circles: experiment; gold triangles: simulation).

NL4

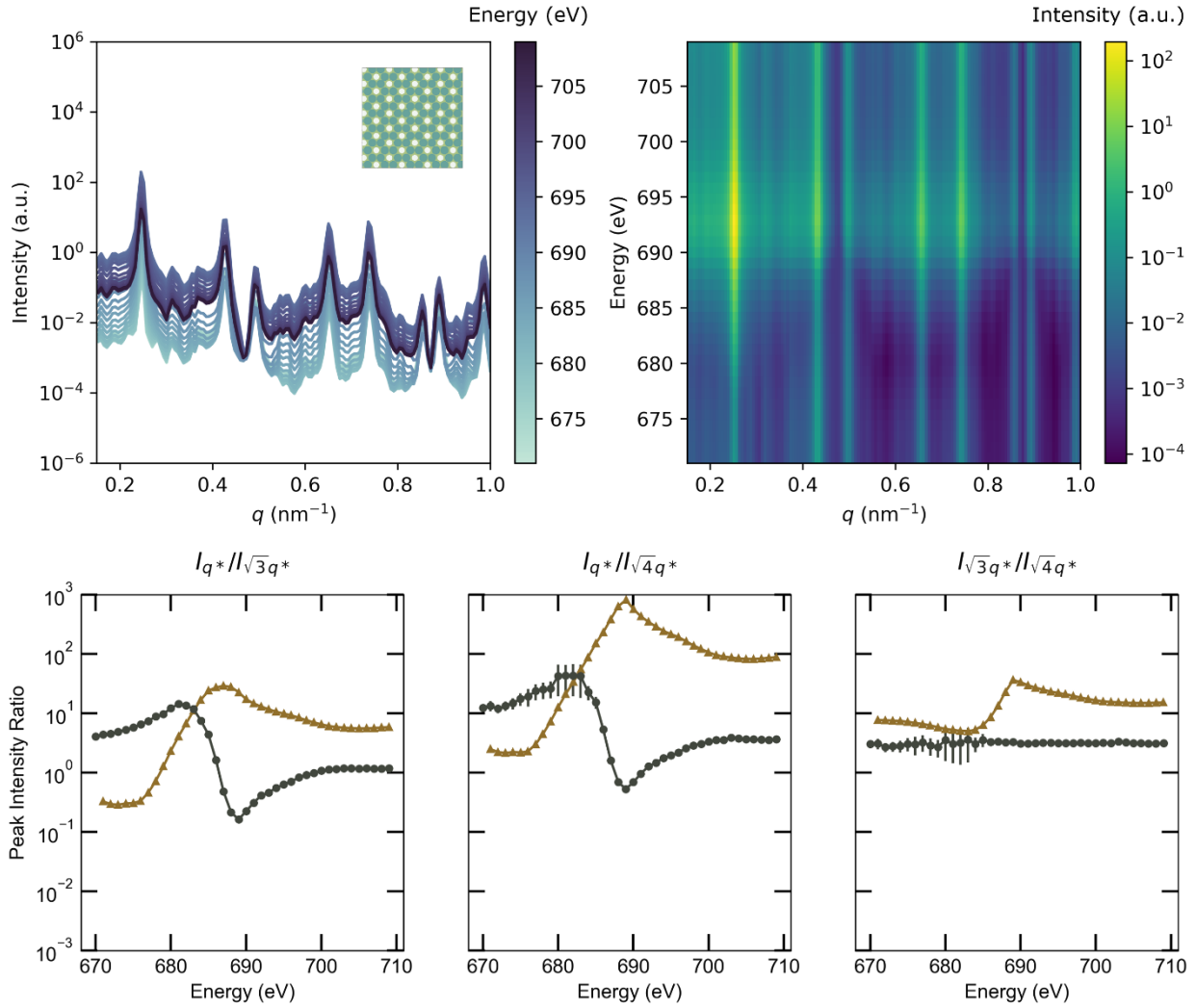


Figure S18. Scattering simulation results for NL4. *Top left:* Radially-averaged simulated RSoXS profiles at energies along the F edge (*inset:* 200 × 200 voxel subset of the model); *Top right:* intensity map of the simulated RSoXS profiles; *Bottom:* energy dependence of peak intensity ratios (dark grey circles: experiment; gold triangles: simulation).

NL5

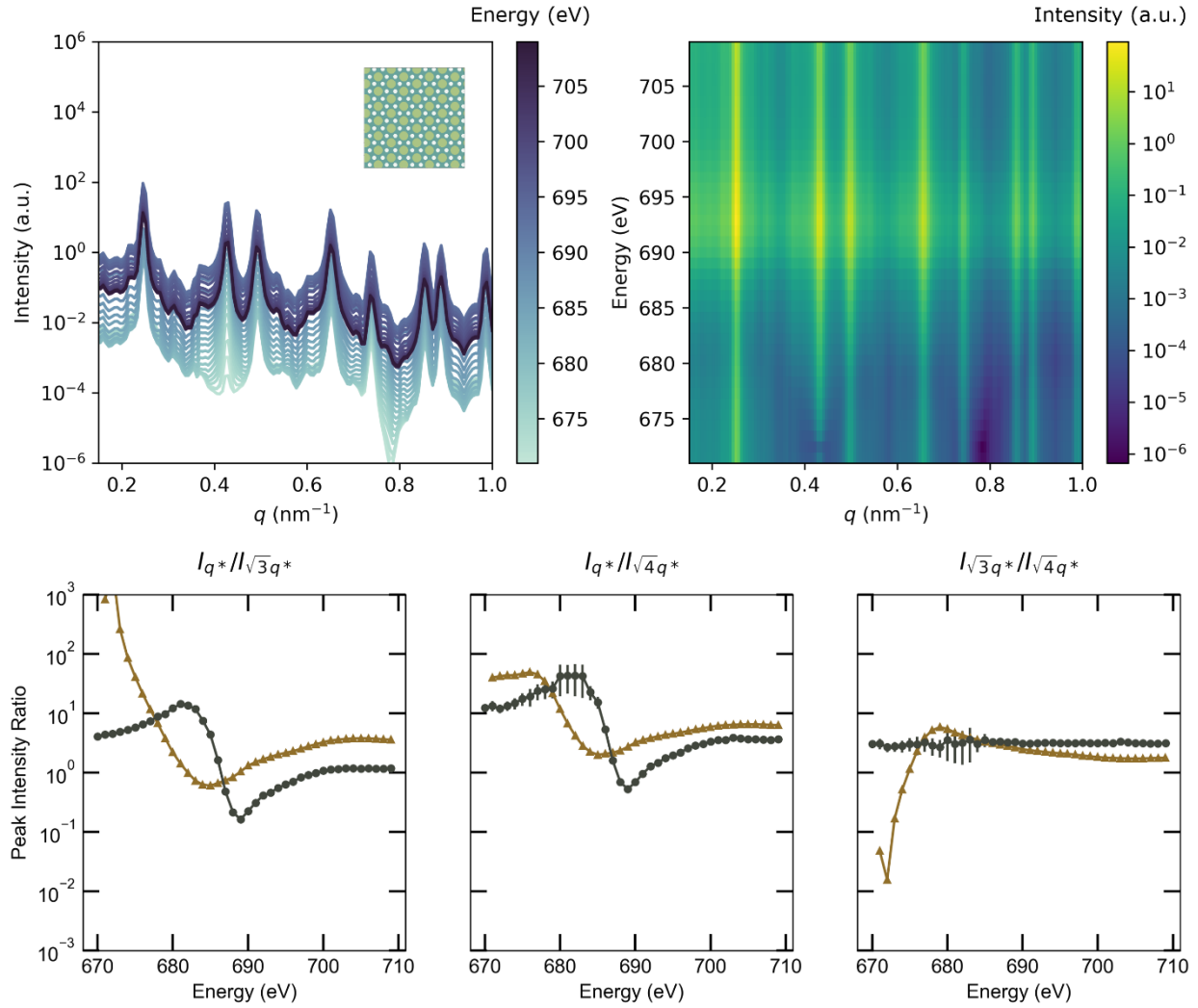


Figure S19. Scattering simulation results for NL5. *Top left:* Radially-averaged simulated RSoXS profiles at energies along the F edge (*inset:* 200×200 voxel subset of the model); *Top right:* intensity map of the simulated RSoXS profiles; *Bottom:* energy dependence of peak intensity ratios (dark grey circles: experiment; gold triangles: simulation).

NL6

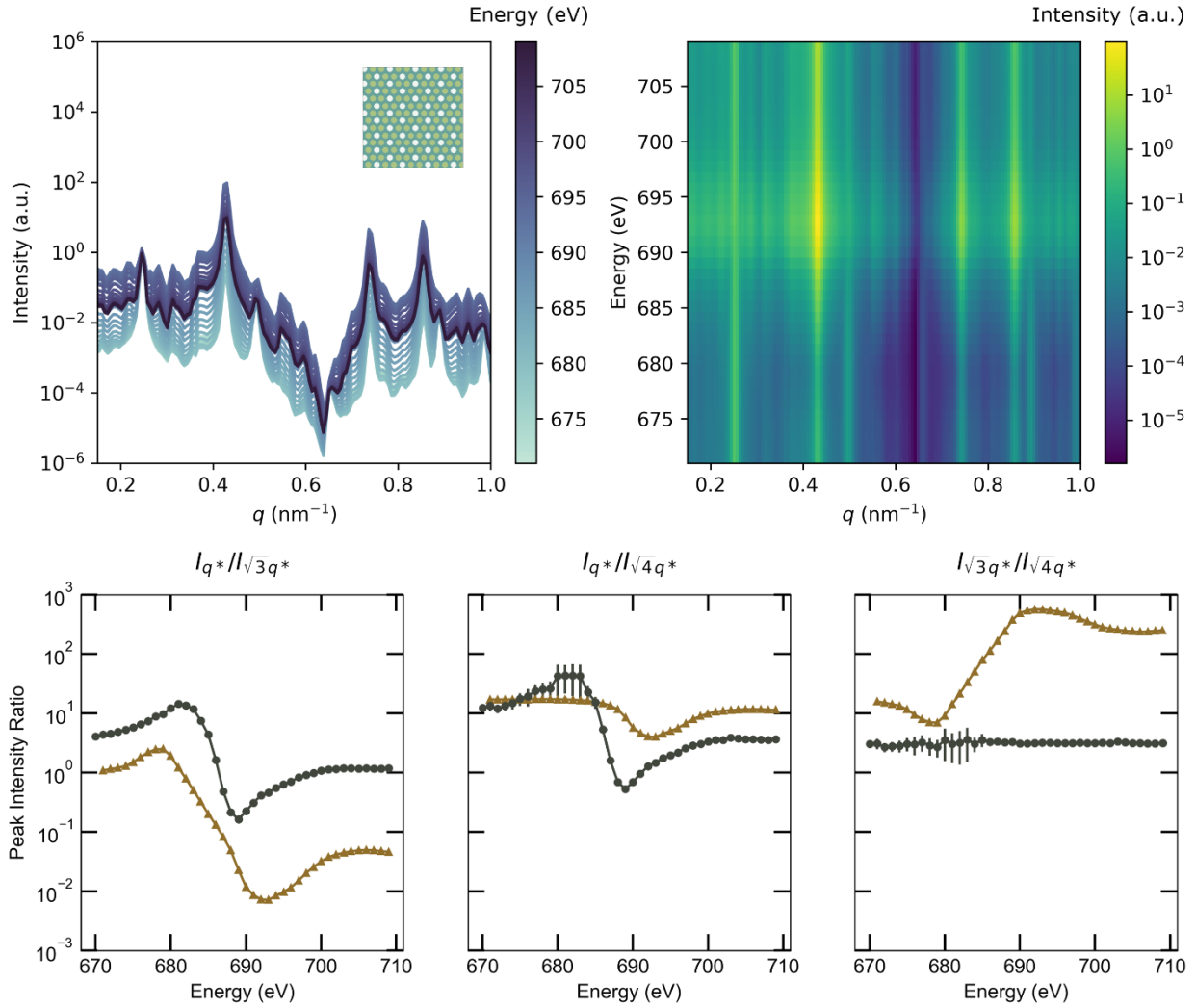


Figure S20. Scattering simulation results for NL6. *Top left:* Radially-averaged simulated RSoXS profiles at energies along the F edge (*inset:* 200 × 200 voxel subset of the model); *Top right:* intensity map of the simulated RSoXS profiles; *Bottom:* energy dependence of peak intensity ratios (dark grey circles: experiment; gold triangles: simulation).

Relative root-mean-squared error (RRMSE) calculation

The goodness-of-fit between experimental and simulated peak intensity ratios was evaluated using relative root-mean-squared error (RRMSE) of the natural logarithm of the ratios:

$$y = \ln(\text{ratio})$$

$$RMSE = \sqrt{\frac{1}{N} \sum_{i=1}^N (y_{exp} - y_{sim})^2}$$

$$RRMSE = \frac{RMSE}{\sqrt{\frac{1}{N} \sum_{i=1}^N (y_{exp} - \overline{y_{exp}})^2}}$$

Impact of cylinder orientation

The scattering simulations represent cylinders oriented perpendicular to the substrate, but experimental samples may contain grains of cylinders oriented in many different directions relative to the substrate. We explored the impact of orientation by integrating the analytical expression for the particle form factor $P(q)$ of a cylinder⁶ over different angular ranges. Relative to an isotropic distribution of cylinder orientations, perpendicular cylinders have a form factor which is lower in overall magnitude, higher in amplitude (difference between maximum and minimum values), and similar with respect to the locations of the minima in q -space. We expect that these differences could cause the magnitude of our simulated intensity ratios to be off relative to a typical (polycrystalline) experimental sample, but that the line shape of the ratios vs. energy will be similar.

$J_1(x)$ = first order Bessel function of the first kind

R = cylinder radius

L = cylinder length

α = angle between the cylinder axis and the scattering vector ($\alpha = \frac{\pi}{2}$ for cylinders oriented perpendicular to the substrate)

$$P(q) = \int_{\alpha_1}^{\alpha_2} \left[\frac{2 \cdot J_1(q \cdot R \cdot \sin \alpha)}{q \cdot R \cdot \sin \alpha} \cdot \frac{\sin((q \cdot L \cdot \cos \alpha)/2)}{(q \cdot L \cdot \cos \alpha)/2} \right]^2 \sin \alpha \, d\alpha$$

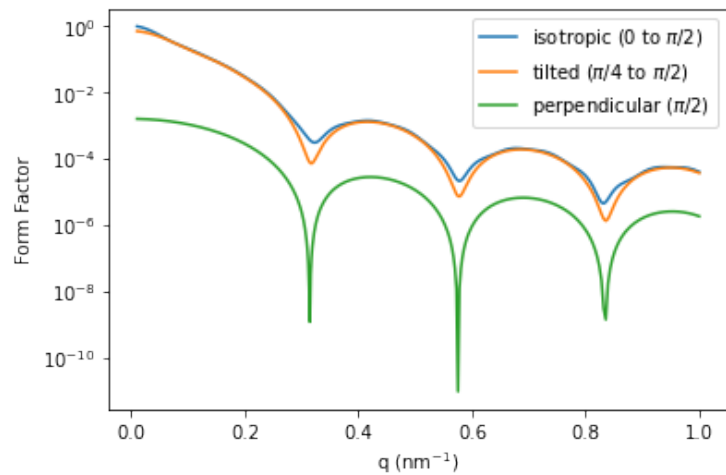


Figure S21. Calculated particle form factor for cylinders with varying orientation distributions.

References

- 1 A. Watts, N. Kurokawa and M. A. Hillmyer, *Biomacromolecules*, 2017, **18**, 1845–1854.
- 2 M. A. White, J. A. Johnson, J. T. Koberstein and N. J. Turro, *J. Am. Chem. Soc.*, 2007, 129, 4504.
- 3 H. Ade and S. Urquhart, in *Chemical Applications of Synchrotron Radiation Part I: Dynamics and VUV Spectroscopy*, ed. T.-K. Sham, World Scientific Publishing Co., 2002, pp. 285–355.
- 4 J. Ilavsky, *J. Appl. Crystallogr.*, 2012, **45**, 324–328.
- 5 M. Newville and T. Stensitzki, *Non-Linear Least-Squares Minimization and Curve-Fitting for Python*, 2018, 65.
- 6 P. Lindner and T. Zemb, Eds., *Neutrons, X-rays and light : scattering methods applied to soft condensed matter*, Elsevier, Amsterdam, 1st ed., 2002.